

Seasonal and interannual variability of satellite-derived chlorophyll pigment, surface height, and temperature off Baja California

T. Leticia Espinosa-Carreón,¹

Centro de Investigación Científica y de Educación Superior de Ensenada, Baja California, Mexico

P. T. Strub

College of Oceanic and Atmospheric Sciences, Oregon State University, Corvallis, Oregon, USA

Emilio Beier,¹ Francisco Ocampo-Torres, and Gilberto Gaxiola-Castro

Centro de Investigación Científica y de Educación Superior de Ensenada, Baja California, Mexico

Received 22 August 2003; revised 19 December 2003; accepted 23 January 2004; published 24 March 2004.

[1] Mean fields, seasonal cycles, and interannual variability are examined for fields of satellite-derived chlorophyll pigment concentrations (CHL), sea surface height (SSH), and sea surface temperature (SST) during 1997–2002. The analyses help to identify three dynamic regions: an upwelling zone next to the coast, the Ensenada Front in the north, and regions of repeated meanders and/or eddy variability west and southwest of Point Eugenia. High values of CHL are found in the upwelling zone, diminishing offshore. The exception is the area north of 31°N (the Ensenada Front), where higher CHL are found about 150 km offshore. South of 31°N, the long-term mean dynamic topography decreases next to the coast, creating isopleths of height parallel to the coastline, consistent with southward geostrophic flow. North of 31°N the mean flow is toward the east, consistent with the presence of the Ensenada Front. The mean SST reveals a more north-south gradient, reflecting latitudinal differences in surface heating due to solar radiation. Harmonic analyses and EOFs reveal the seasonal and interannual patterns, including the region of repeated eddy activity to the west and southwest of Point Eugenia. A maximum CHL occurs in spring in most of the inshore regions, reflecting the growth of phytoplankton in response to the seasonal maximum in upwelling-favorable winds. SST and SSH anomalies are negative in the coastal upwelling zone in spring, also consistent with a response to the seasonal maximum in upwelling. When the seasonal cycle is removed, the strongest signal in the EOF time series is the response to the strong 1997–1998 El Niño, with a weaker signal representing La Niña (1998–1999) conditions. El Niño conditions consist of low chlorophyll, high SSH, and high SST, with opposite conditions during La Niña. **INDEX TERMS:** 4223 Oceanography: General: Descriptive and regional oceanography; 4227 Oceanography: General: Diurnal, seasonal, and annual cycles; 4275 Oceanography: General: Remote sensing and electromagnetic processes (0689); **KEYWORDS:** chlorophyll, El Niño, La Niña, Baja California, California Current

Citation: Espinosa-Carreón, T. L., P. T. Strub, E. Beier, F. Ocampo-Torres, and G. Gaxiola-Castro (2004), Seasonal and interannual variability of satellite-derived chlorophyll pigment, surface height, and temperature off Baja California, *J. Geophys. Res.*, 109, C03039, doi:10.1029/2003JC002105.

1. Introduction

[2] In this paper, we examine the links between physical forcing and the lower trophic levels off Baja California, in the southern part of the California Current System (CCS). The mean flow in the CCS is equatorward next to the coast in the Northeast Pacific Ocean [Hickey, 1979, 1998]. It is

delimited at its northern boundary by the eastward North Pacific Current, which divides the Subtropical Gyre from the Subarctic Alaska Gyre. At its southern extreme, the CCS flows into the westward North Equatorial Current [Parés-Sierra *et al.*, 1997]. At the most basic level, the flow of the California Current is controlled by the equatorward current needed to complete the Subtropical Gyre and by the predominantly equatorward winds. This area is considered to be an oceanographic transitional zone between midlatitude and tropical ocean conditions [Durazo and Baumgartner, 2002].

[3] The CCS is often depicted as a prototype eastern boundary current (EBC), with a 2-D upwelling structure

¹Also at College of Oceanic and Atmospheric Sciences, Oregon State University, Corvallis, Oregon, USA.

consisting of offshore Ekman transport at the surface and subsurface onshore return flow. An equatorward jet forms at the offshore edge of the upwelled water, which is cold, salty, and rich in nutrients. These nutrients lead to an increase in primary production, which provides the basis for a productive ecosystem.

[4] Unlike the simple 2-D patterns depicted in most textbooks, however, synoptic circulation patterns observed in the CCS and other EBCs are characterized by complex mesoscale eddies, fronts, and meanders, with horizontal scales from tens to hundreds of kilometers [Pelaéz and McGowan, 1986]. This structure develops seasonally and varies on interannual and longer scales [Pelaéz and McGowan, 1986; Strub *et al.*, 1991]. In this paper, we use satellite observations of chlorophyll pigment concentration, sea surface height, and temperature to illustrate the space and time relationships between biological and physical processes off Baja California. This region has been previously described by Gómez-Valdés and Vélez-Muñoz [1982], Parés-Sierra *et al.* [1997] and Durazo and Baumgartner [2002]. The analysis in this paper also builds on previous work using in situ and satellite chlorophyll estimations from Bernal [1981], Pelaéz and Guan [1982], Pelaéz and McGowan [1986], Strub *et al.* [1990], Thomas and Strub [1990], Fargion *et al.* [1993], Thomas *et al.* [1994], Hayward *et al.* [1999], Kahru and Mitchell [2000, 2001, 2002], Bograd *et al.* [2000], and Durazo *et al.* [2001].

2. Data and Methods

2.1. Chlorophyll

[5] SeaWiFS (Sea Viewing Wide Field of View Sensor) ocean color data were provided by A. Thomas at the University of Maine. After initial processing [Barnes *et al.*, 1994], 8-day and monthly composites were remapped with 4-km resolution. The period chosen for study extends from September 1997 (the beginning of the available data) to May 2002; the region is 22°N–33°N and 112°W–120°W (Figure 1).

2.2. Sea Surface Height (SSH)

[6] SSH data were formed from a combination of TOPEX and ERS-2 altimeters, using data from January 1997 to November 2001 (when the TOPEX satellite was moved to a new orbit), over the same region as used for SeaWiFS chlorophyll pigment concentrations. These data were processed and made available by the NOAA-NASA Pathfinder Project [Strub and James, 2002], using standard atmospheric corrections. In order to combine the data from the two altimeters, the spatial mean over the domain of interest for each altimeter is first removed for each month. This removes offsets between the two altimeters caused by residual orbit errors, and it also removes the dominant seasonal cycle, which is the rise and fall of SSH caused by the seasonal heating cycle. What remains is the temporal and spatial variability in SSH gradients, which is the dynamical signal of interest. To partially compensate for the loss of the temporal mean height field (which is removed along with the unknown marine geoid), a climatological mean dynamic-height field (relative to 500 m) is formed from the long-term mean temperature and salinity

fields of Levitus *et al.* [1998] (Figure 2b) and added to the spatial EOF patterns for altimeter SSH. There is some question about the spatial “resolution” of SSH fields formed from combinations such as this. We take the scale of resolution to be approximately 100–200 km, but in analyses such as these, using temporal means, harmonic analyses and EOFs, small-scale noise is reduced and only the dominant larger-scale features are preserved.

2.3. Sea Surface Temperature (SST)

[7] The several clearest images from each week were used to form “warmest-pixel” fields of SST from the NOAA-14 Advanced Very High Resolution Radiometer (AVHRR), between January 1997 and May 2002. Monthly means were calculated from these weekly fields. Nominal spatial resolution of the remapped SST data is 1.2 km. Multichannel SST algorithms were similar to those used by the NOAA-NASA Pathfinder project.

2.4. Wind Stress and the Coastal Upwelling Index

[8] Temporal variability in the upwelling intensity over Baja California is quantified by the Coastal Upwelling Index (CUI), produced by the NOAA/NMFS Pacific Fisheries Environmental Laboratory in Monterey, California [Bakun, 1975; Schwing *et al.*, 1996]. We use the CUI time series centered on 27°N and 116°W (Figure 1) as representative of the Baja California region. The period for the data is from January 1997 to May 2002. To characterize the spatial patterns of seasonal wind stress, we use winds from the European Centre for Medium-Weather Forecasts (ECMWF), from January 1986 to January 1998.

2.5. Seasonal Cycle

[9] Seasonal cycles of chlorophyll, SSH, SST, wind stress, and the CUI are calculated by fitting the time series to a mean plus annual and semiannual harmonics,

$$F(\bar{x}, t) = A_0(\bar{x}) + A_1(\bar{x}) \cos(\omega t - \varphi_1) + A_2(\bar{x}) \cos(2\omega t - \varphi_2) \quad (1)$$

where A_0 , A_1 , and A_2 are the temporal mean, annual amplitude, and semiannual amplitude for each time series, respectively; $\omega = 2\pi/365.25$ is the annual radian frequency; φ_1 and φ_2 are the phases of annual and semiannual harmonic respectively; and t is the time (as year-day). Mean fields were obtained for all data, except for SSH, where the long-term mean of the altimeter SSH must be removed to eliminate the marine geoid. The long-term mean of dynamic height is derived from the Levitus *et al.* [1998] climatology with reference of 500 dbar (Figure 2b).

[10] In the analysis below, we refer to “seasonal anomalies” as the sum of the second and third terms of the right-hand of equation (1). “Nonseasonal anomalies” are the time series after removing the temporal mean, annual and semiannual cycles as in equation (1). Empirical Orthogonal Functions (EOFs) are presented for both seasonal and nonseasonal anomalies. After the EOF modes of SSH are obtained from the data with the long-term mean removed, the long-term mean dynamic height derived from Levitus *et al.* [1998] is added to partially make up for the loss of the mean circulation. For consistency, we show the first three EOF modes of all parameters, although their statistical

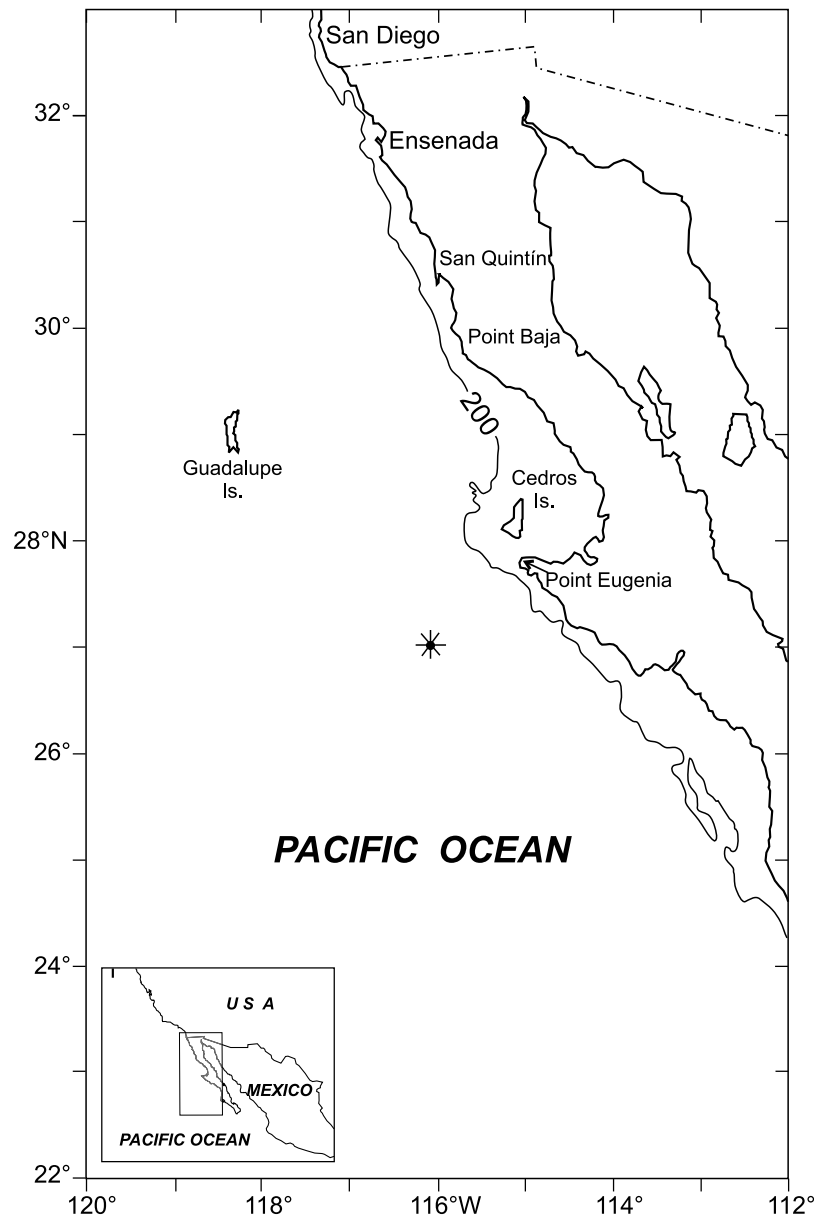


Figure 1. Study area, with isobaths of 200 m. The location of the Coastal Upwelling Index (CUI) is indicated by the asterisk located at 27°N, 116°W, selected as a representative of the Baja California region.

significance varies between CHL, SST, and SSH. Regardless of formal statistical certainty, the patterns are generally interpretable in terms of expected mesoscale dynamics.

3. Results and Discussion

3.1. Mean Fields

[11] The mean chlorophyll pigment concentrations are greatest in an alongshore band next to the coast, approximately 50–100 km wide (Figure 2a), except north of 31°N, where the pigment concentrations are higher offshore. The eutrophic nearshore region (chlorophyll $>1 \text{ mg m}^{-3}$) has been previously described by Kahru and Mitchell [2000], along with the oligotrophic offshore ocean (chlorophyll $<0.2 \text{ mg m}^{-3}$) and the mesotrophic intermediate zone (chlorophyll $\sim 0.2\text{--}1.0 \text{ mg m}^{-3}$). The mean SSH field

(Figure 2b) calculated from climatological temperatures and salinities [Levitus *et al.*, 1998] slopes downward toward the coast as expected for equatorward flow [Simpson *et al.*, 1986]. South of 31°N, both pigment and SSH are consistent with the equatorward mean wind stress (Figure 3a), which is upwelling-favorable. The mean field of SST shows strong north-south gradients, with isopleths approximately perpendicular to the coast in the southern region (Figure 2c). SST diminishes from about 21°C in the southeast to $\sim 17^\circ\text{C}$ off northwest Baja California, as also reported by Lynn *et al.* [1982]. Temperatures are 3°–5°C higher than reported by Gallaudet and Simpson [1994], however, due to the presence of the 1997–1998 El Niño in our data set and the larger domain considered. The northern part of the pigment and SST, and SSH fields in Figure 2 show a strong north-south gradient associated with the “Ensenada Front”

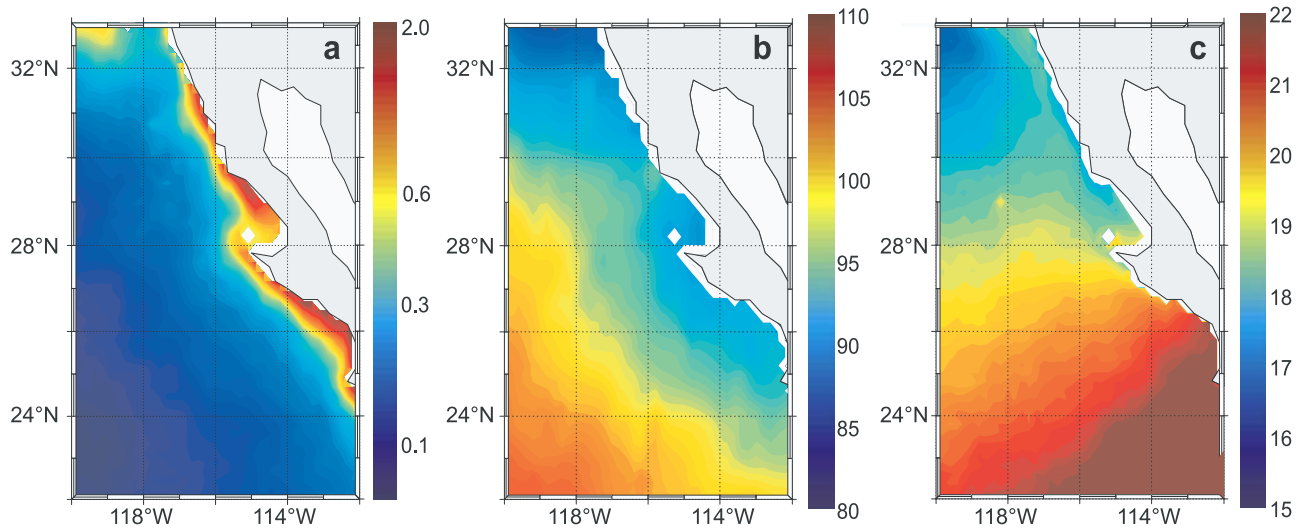


Figure 2. (a) Temporal mean chlorophyll concentration (mg m^{-3}) field, (b) long-term mean dynamic topography (cm) with reference to 0/500 dbar, derived from *Levitus et al.* [1998] climatology, and (c) temporal mean of the sea surface temperature ($^{\circ}\text{C}$) fields.

near 32°N . The front separates colder water with higher pigments to the north from warmer, less productive water in the southern part of the Southern California Bight [*Gaxiola-Castro and Alvarez-Borrego*, 1991; *Haury et al.*, 1993].

[12] The mean wind stresses (1986–1998) derived from ECMWF are depicted in Figure 3a, which shows mainly southeastward wind stress over the ocean, parallel to the coast and favorable for upwelling in coastal areas. The low SSH north of 31°N depict the cyclonic circulation expected in the southern part of the Southern California Bight, associated with low temperatures and high pigment concentrations offshore. Over this area, the mean vertical

component of the wind stress curl is positive and large, as indicated by the decreasing southward winds as one moves toward the coast. The positive curl may contribute to the cyclonic circulation in this region.

3.2. Seasonal Cycles

[13] The seasonal ECMWF wind stress anomalies during April and October are presented in Figure 3. These are simple averages of all Aprils and Octobers during the 13-year time series after removing the long-term mean, rather than a reconstruction from harmonics. A harmonic reconstruction would look nearly identical, since the 13-year time series is long enough for the simple means to represent

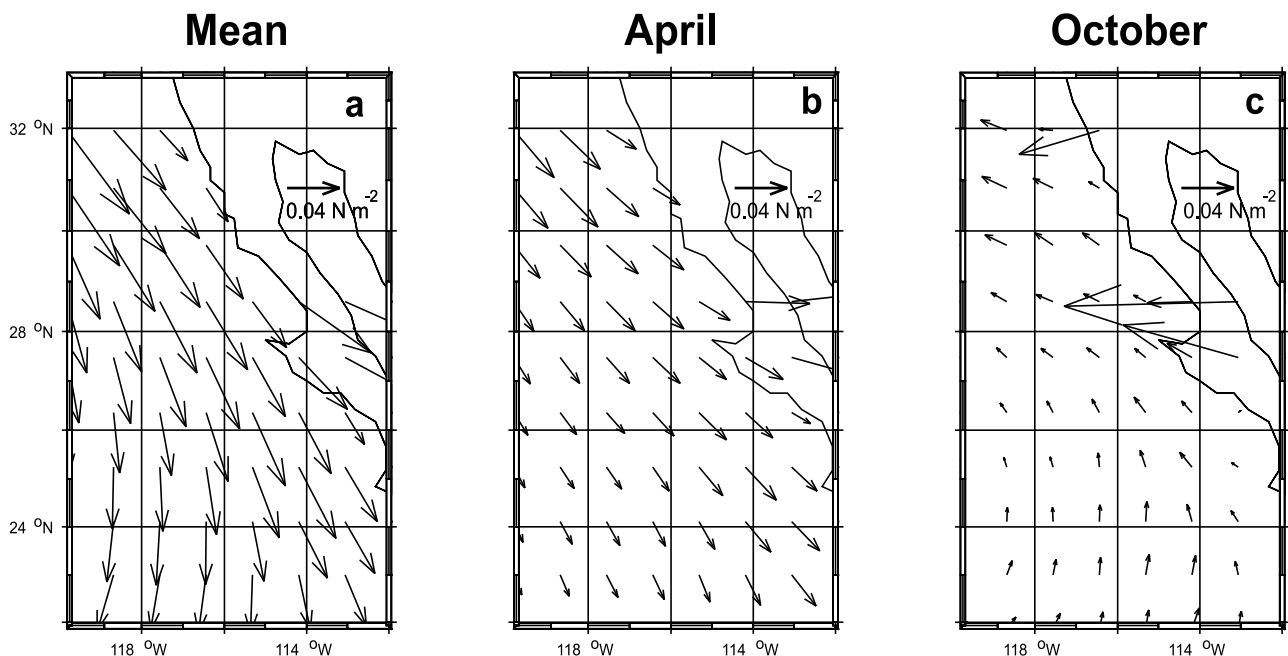


Figure 3. (a) Temporal mean (1986–1998) field of wind stress (N m^{-2}), and spatial pattern for the seasonal anomalies of wind stress (N m^{-2}) for (b) April and (c) October.

the seasonal cycle. The April wind stress anomalies are toward the southeast, similar to and reinforcing the temporal mean (the maximum in upwelling-favorable winds is approximately at this time). In contrast, the October wind stress anomalies are toward the northwest, representing a decrease in the upwelling-favorable winds, but not a reversal over the ocean.

[14] Similar seasonal anomalies of chlorophyll, SSH, and SST are reconstructed from the harmonic fits in Figure 4. As for winds, the April and October fields are presented without the temporal mean (Figure 2), to emphasize the seasonal changes. The percentages of the total variance explained by the harmonic fits at each location are shown Figures 4c, 4f, and 4i.

[15] Maximum amplitudes of the pigment seasonal cycles for most locations are approximately 0.5 mg m^{-3} , largest next to the coast and near zero in offshore regions. The negative seasonal anomalies in October combine with the nearshore mean field (values of 0.6 mg m^{-3} or more) to reduce pigment concentrations to near zero. The variance explained by the pigment seasonal cycles next to the coast in the primary upwelling regions reaches values between 45% to 65% (Figure 4c), largest south of Points Eugenia and Baja.

[16] The magnitudes of the SSH seasonal cycles reach values of 6 cm, and these are not restricted to the coastal upwelling regions. Rather, the pattern south of 28°N in April shows high offshore SSH when the coastal ocean has low SSH. The opposite pattern occurs south of 30°N in October. Combined with the mean SSH field in Figure 2b, these fields describe strong equatorward flow in spring and weak or reversed flow in fall. This timing is consistent with a maximum in upwelling-favorable wind stress (Figure 3b) that occurs earlier off Baja California than in the rest of the California Current farther north [Huyer, 1983; Lynn and Simpson, 1987].

[17] The high seasonal variability in the offshore SSH fields is not the usual seasonal variability in steric heights that is typical of altimeter fields. This seasonal steric signal is mostly removed when we subtract the spatial mean from each altimeter data set (TOPEX/Poseidon or ERS-2) before combining them to form monthly SSH fields. Rather, these patterns are associated with persistent meanders and eddies in the flow field that reoccur on a seasonal timescale at preferred locations. Previous studies of the California Current farther north have documented similar meanders and eddies and have related them to three processes: wind-forcing, instabilities of the coastal flow (barotropic and baroclinic), and coastal geometry [Ikeda and Emery, 1984; Narimousa and Maxworthy, 1989; Simpson and Lynn, 1990; Strub et al., 1991; Abbott and Barksdale, 1991; Haidvogel et al., 1991; Parés-Sierra et al., 1993; Barth et al., 2000].

[18] Off Baja California, we expect similar processes to create eddies and meanders, and Soto-Mardones et al. [2004] suggest that the geometry of the coastline is one of the primary mechanisms of eddy generation off Baja California (the other is the interaction of the cool, equatorward California Current at the surface and the poleward California Undercurrent). A particularly strong pair of features in SSH is found west of Point Eugenia, where in April, there is a region of low SSH north of high SSH (opposite in October). This indicates a tendency for cyclonic

meanders north of Point Eugenia in April (when currents are strongest), with anticyclonic meanders west/southwest of the point. While the seasonal harmonics explain only 10–15% of the variance over much of the region, they explain 25–40% of the variance in the SSH feature west-southwest of Point Eugenia (high SSH in April and low SSH in October). Thus this is a regularly reoccurring meander and appears related to the location of Point Eugenia. The other locations where the harmonic fits explain 25–40% of the variance include southern coastal regions and the core of the CCS north of the Ensenada Front (Figure 4f).

[19] Why are there no increased pigment concentrations associated with the shoaling of the thermocline in offshore cyclonic eddies, as described by McCarthy et al. [2002]? The most likely explanation is that offshore surface nutrients are depleted, offshore stratification is strong, and the nutricline is too deep for the geostrophically raised pycnocline in cyclonic eddies to bring nutrients to within the euphotic zone.

[20] The amplitudes of the harmonic fits to the SST fields produce maximum values of $\pm 3^\circ\text{C}$, concentrated next to the coast south of Point Eugenia (Figures 4g and 4h). This is easier to see in the October SST field. Thus the harmonic cycles create the onshore-offshore gradients (south of 30°N), which are expected for upwelling systems, but are mostly missing in the mean field. This indicates that the mean fields are primarily created by surface heating processes, with strong latitudinal gradients, while the seasonal variability is controlled by internal processes such as vertical advection (coastal upwelling) and horizontal advection [Parés-Sierra et al., 1997]. Off northern Baja California, the seasonal SST range is reduced to 1°C .

[21] The variance explained by the harmonic seasonal cycle of SST (Figure 4i) is lowest in a narrow band next to the coast (45–50%) from Point Eugenia to the north. Offshore of this narrow band, the variance explained is generally more than 65–70%, except in a band extending to the southwest off Point Eugenia, where eddies may exert more influence. These coastal and offshore bands where the harmonic fits explain less variance imply greater nonseasonal “noise” in the monthly SST fields. This could be caused by the combination of short timescales for the upwelling and eddy SST signals, coupled with irregular cloud cover, which causes the monthly “averages” to be unduly influenced by sporadic sampling. These short timescales are in contrast to the long timescales of strong seasonal warming and cooling, which dominate the monthly means over most of the domain (where upwelling and eddies are not present).

[22] Focusing on the inshore region, an inverse relationship is found between SSH and chlorophyll (Figures 4a, 4b, 4d, and 4f). The low SSH and high pigments are consistent with coastal upwelling and equatorward flow in early spring. These processes together produce cold (low steric height) and nutrient-rich inshore waters, increasing phytoplankton growth. The opposite conditions are found during fall, when the poleward flow is present and warm and nutrient-poor water dominates the inshore conditions. Both scenarios are consistent with the wind stress seasonal anomalies during April and October (Figures 3b and 3c).

[23] A second region of interest is the offshore Ensenada Front (32°N – 33°N , 118°W – 120°W), where an area of high

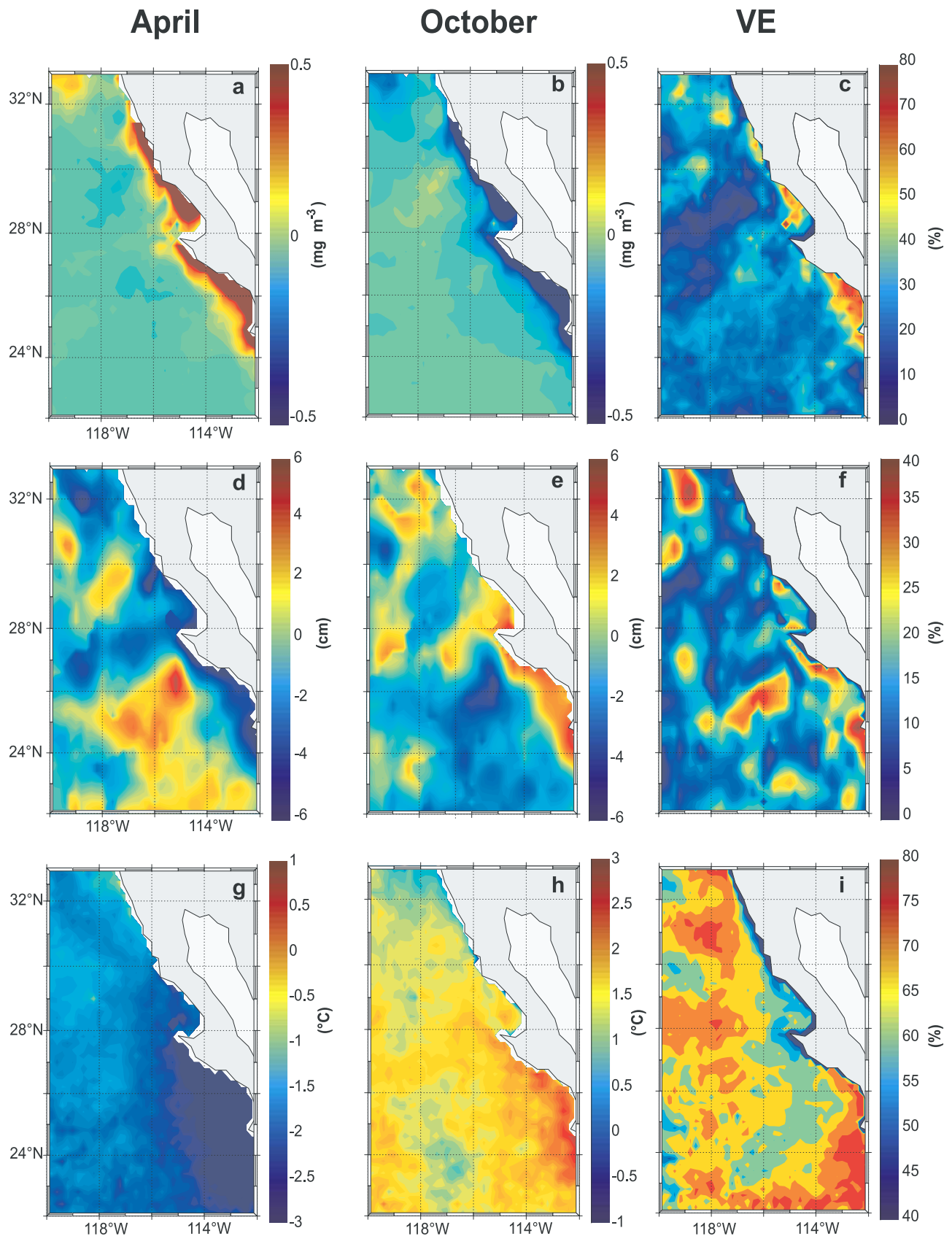


Figure 4. Spatial patterns for seasonal anomalies of chlorophyll, SSH, and SST for April and October, reconstructed from the annual and semiannual fits. Chlorophyll (mg m⁻³): (a) April, (b) October, and (c) percent of variance explained. Sea surface height (cm): (d) April, (e) October, and (f) percent of variance explained. Sea surface temperature (°C): (g) April, (h) October, and (i) percent of variance explained.

(low) chlorophyll concentration (Figures 4a and 4b) is associated with low (high) SSH (Figures 4d and 4e) and SST (Figures 4g and 4h). The lower (high) SSH signal suggest a general cyclonic (anticyclonic) circulation that develops during April (October). The cyclonic (anticyclonic) circulation produces shoaling (deepening) of isopycnals that may act to increase nutrient supply to the euphotic zone, promoting (reducing) phytoplankton growth [McCarthy *et al.*, 2002]. Although high chlorophyll concentrations in the Ensenada Front during spring and summer have been described by Peláez and McGowan [1986] based on CZCS color data, the front is thought to be a zone of convergence between the California Current and the Central Pacific intrusion, which should be low in nutrients and phytoplankton [Hickey, 1979; Haury *et al.*, 1993; McGowan *et al.*, 1996]. Previous studies of the Ensenada Front using shipboard data do not suggest enhanced production or accumulation of biomass [Venrick, 2000]. However, our results demonstrate an inverse relation between chlorophyll pigment and SSH, implying a role for a shallow pycnocline. This does not rule out a role for advection of biomass into the Ensenada Front region, which we cannot address. The front is less obvious in the SST fields in April, which shows the cold core of the California Current stretching from 33°N, 120°W to the southeast.

[24] In summary, Figures 2–4 reveals a mix of several mesoscale processes that create the patterns in surface pigment concentrations, SST, and SSH. Coastal upwelling creates low SSH and SST along with high pigment concentrations in a band next to the coast south of approximately 31°N. This upwelling is driven by the seasonal winds, with a maximum around April. An equatorward jet develops along the gradient in SSH. Eddies and meanders in the current are most likely generated by barotropic and baroclinic instabilities [Ikeda and Emery, 1984; Olson, 2002]. More persistent cyclonic and anticyclonic eddies appear off Point Eugenia and in the Southern California Bight (perhaps with a contribution in the bight from positive wind stress curl). The low SSH in the cyclonic eddy in the bight, north of the Ensenada Front, is associated at least sometimes with higher pigment contributions, suggesting changes in nutrient depth as a possible mechanism. The fact that the relatively strong offshore features in SSH are not associated with offshore signals over most of our region is probably due to the high static stability and lack of nutrients in the offshore water. The mostly north-south gradient in the mean SST field is consistent with a dominance at the surface of surface heating fields. The east-west SST gradient in the seasonal changes reflects the seasonal occurrence of upwelling/downwelling. Upwelling/downwelling events have timescales shorter than seasonal, as revealed by the low amount of SST variance explained by the seasonal cycles in a coastal band north of 27°N.

3.3. Seasonal and Nonseasonal Anomalies in Coastal Upwelling Index (CUI)

[25] In Figure 5a we present the seasonal anomalies of the CUI at 27°N, 116°W for the period from January 1997 to May 2002. The seasonal fit to annual plus semiannual harmonics is also shown. This fit has a semiannual periodicity, with a primary yearly maximum in spring (April–May) and a primary minimum in late summer

(August–September). Secondary maximum and minimum values occur in autumn (October–November) and winter (January–February). The timing of these maxima are similar to the semiannual peaks in alongshore geostrophic transport found by Chelton [1984] at several locations off central and southern California. The very negative September 1997 CUI value was caused by Hurricane Nora. Strong positive values of the CUI occurred in April–May 1998, as the 1997–1998 El Niño was ending. Strong upwelling forcing continued to occur in late 1998 and much of 1999. Bograd *et al.* [2000] previously reported anomalously strong upwelling conditions during the 1999 La Niña period. Removing the seasonal cycle in Figure 5b makes the strong upwelling during 1998–1999 even more evident. During 2000–mid-2002, the CUI followed its seasonal cycle more closely, with generally weaker upwelling than during 1998–1999. It is clear that sporadic upwelling can occur at any time of year off Baja California. In comparison to the CUI signal off Oregon (data not shown), there are two differences: the intensity is greater off Oregon (almost 200 metric tons sec⁻¹ 100 m coastline) and it is dominated by the annual periodicity.

3.4. Seasonal and Nonseasonal Anomalies Using EOF Analysis

[26] An alternate view of the seasonal and nonseasonal variability is provided by calculating the EOFs of each data set (for both seasonal and nonseasonal anomalies). The spatial patterns for the first three EOFs of chlorophyll pigments are presented in Figure 6, with their corresponding time series in Figure 7.

[27] The first mode of monthly SeaWiFS pigment concentrations (retaining the seasonal cycle) represents 53% of the total variance (Figures 6a and 7a). In general, harmonic fits represent this mode very well, explaining 79% of the first mode's variance, with a dominant annual periodicity (explaining 42% of the total variance). Maximum pigment concentrations occur in April–July and minimum values are found from October to February. In general, chlorophyll concentrations were lower during and just after the 1998 El Niño period, even with the greater upwelling-favorable winds evident in Figure 5. This is consistent with observations of continued upwelling-favorable forcing during other El Niño periods, during which the deeper pycnoclines keep nutrients below the euphotic zone [Chávez, 1996]. Chlorophyll concentrations rose to above-normal values during the 1999 La Niña and again in 2000. These patterns are even more obvious when the seasonal cycle is removed before calculating the EOF (Figures 6b and 7b). They also agree with the net primary production values estimated for the 0- to 100-km band off southern Baja California by Kahru and Mitchell [2002].

[28] The spatial pattern of the first EOF for pigment concentration is nearly identical to the April pigment field in Figure 4a, with most of the signal in the narrow coastal band. This demonstrates that the first EOF mode isolates most of the seasonal variability. Perhaps more surprising, the first EOF of the nonseasonal anomalies has a nearly identical spatial pattern (Figure 6b) as for seasonal anomalies (Figure 6a). The time series (Figures 7a and 7b) of both first modes suggest that they represent changes in the strength of the summer peaks in pigment concentrations,

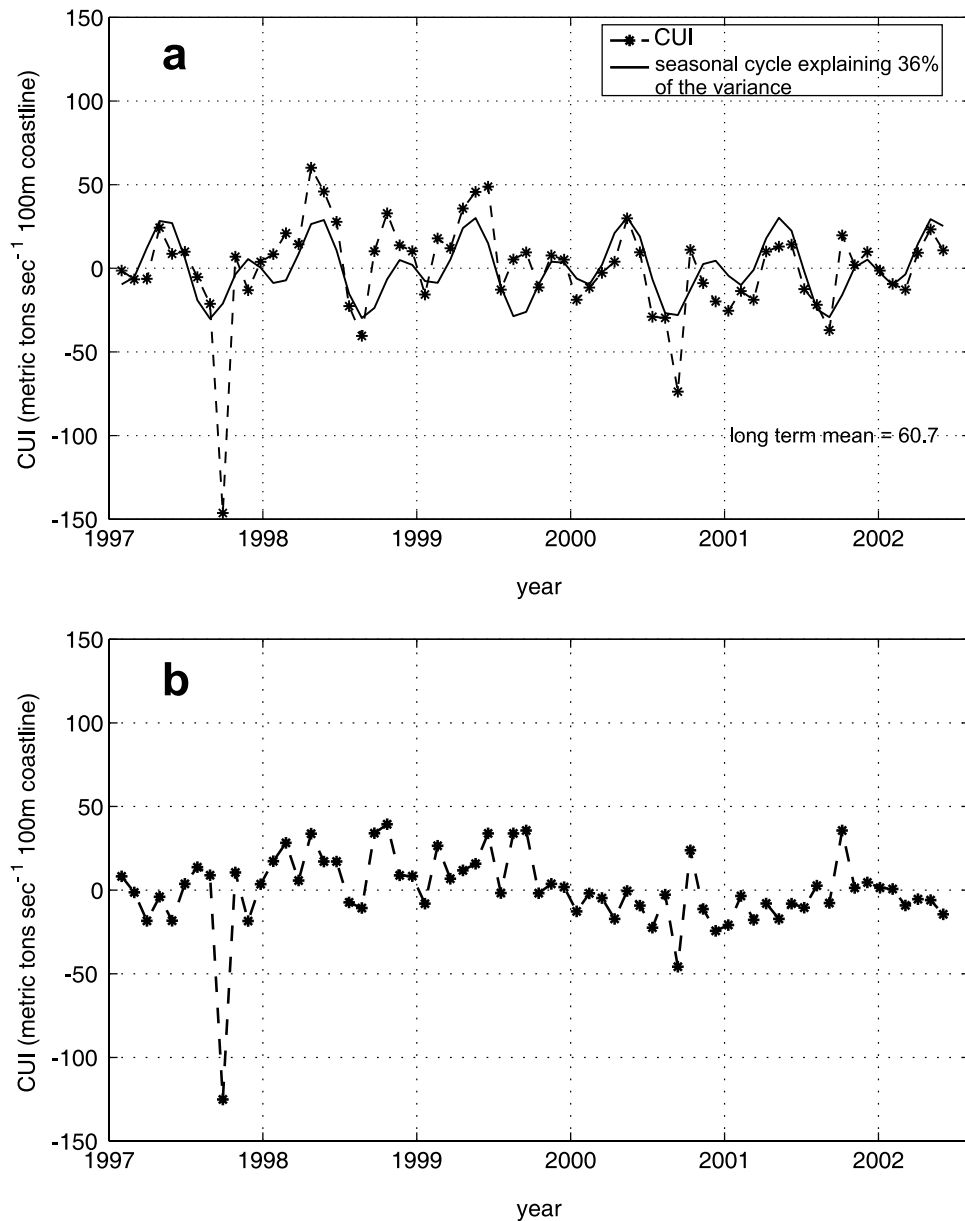


Figure 5. Monthly Coastal Upwelling Index at 27°N, 116°W obtained from the NOAA/NMFS/SWFC Pacific Fisheries Environmental Laboratory in Monterey, California. (a) Seasonal anomalies with the long-term mean removed and showing the fit to annual and semiannual harmonics. (b) Nonseasonal anomalies with the long-term mean removed.

with a weaker peak in 1998 and stronger peaks in 1999 and 2000. Stated differently, the same process that creates the summer peaks in pigment concentrations next to the coast (upwelling and raising of the nutricline next to the coast) produces interannual differences in the strengths of those peaks. Thus signals arriving through either the ocean or atmosphere during the El Niño deepen the nutricline and reduce the effects of coastal upwelling; La Niña conditions may elevate the nutricline and increase the effects of upwelling, but the mechanisms for this process are less clear than for El Niño conditions.

[29] Removal of the seasonal cycles also does not significantly change the spatial patterns of the second and third EOFs of monthly pigment concentrations. These two EOFs

combined explain 16% of the seasonal anomaly variance and 24% of the nonseasonal variance. When all three EOFs are summed, they explain 69% of the total seasonal anomaly variance and the harmonic fits sum to explain 47% of that variance. The second EOF separates the regions north and south of Point Eugenia, while the third EOF isolates specific coastal locations. Negative time series values for the second EOF during mid-1998 indicate the El Niño's greater impact south of Point Eugenia. The relative lack of change in the alongshore locations of maxima and minima when seasonal cycles are removed again argues that the processes which create these alongshore patterns are the same on seasonal and nonseasonal timescales. In this case, Point Eugenia appears to influence the primary alongshore

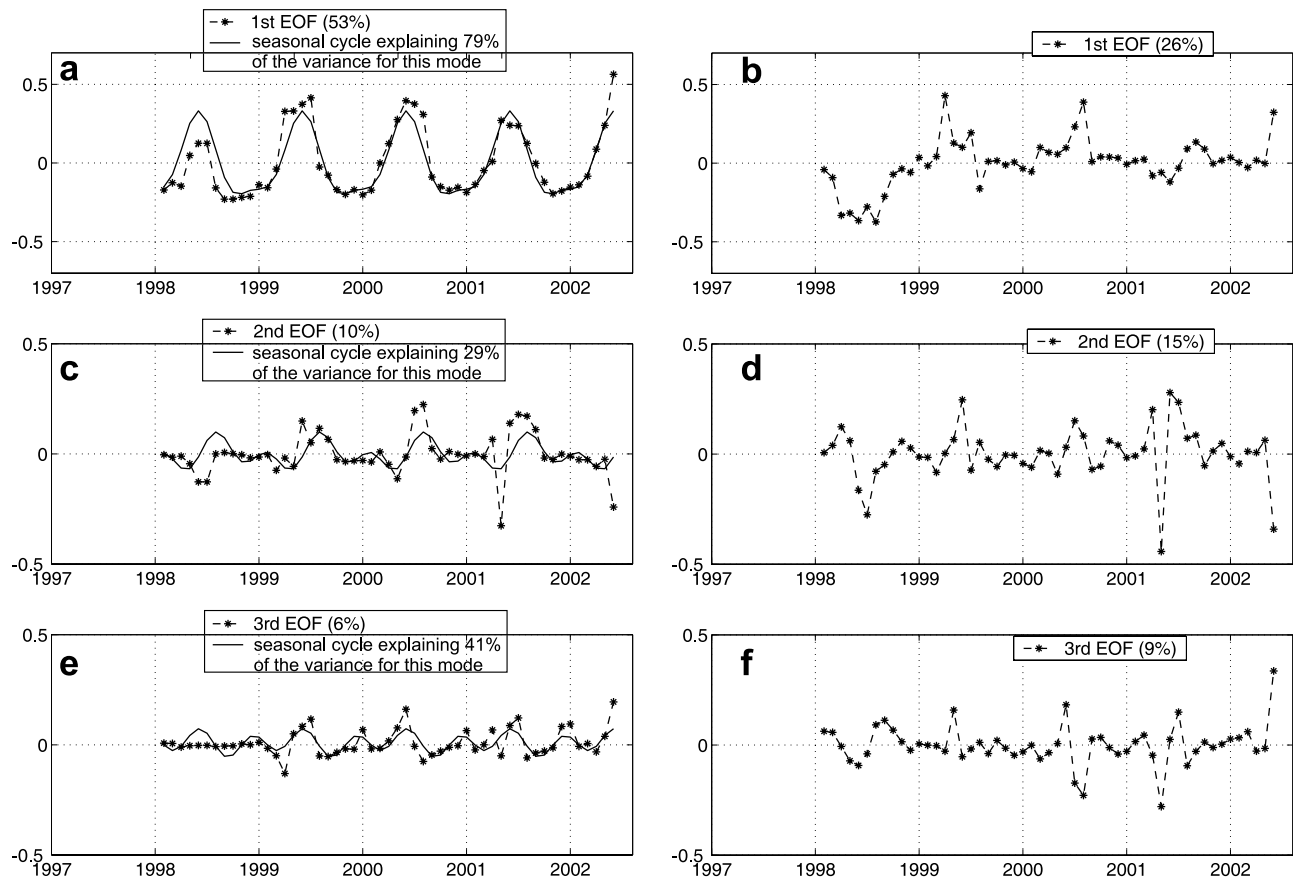


Figure 7. Time series of the first three EOF modes from SeaWiFS chlorophyll concentrations (relative units) from January 1998 to May 2002. First mode with (a) the harmonic seasonal cycle included and (b) the seasonal cycle removed. Second mode with (c) the harmonic seasonal cycle included and (d) the seasonal cycle removed. Third mode with (e) the harmonic seasonal cycle included and (f) the seasonal cycle removed.

pattern of the second EOF, while smaller features of the coastal geometry appear to be associated with the smaller scale alongshore patterns in the second and third EOF.

[30] The first EOF of SSH accounts for 15% of the total variance (Figures 8a and 9a). A fit of harmonics to the first EOF time series gives a seasonal signal that explains 28% of the variance, with a maximum during December–January. We note that the scale of the spatial patterns is between 80 and 120 cm because the long-term mean dynamic height (from Figure 2b) was added to make up for the loss of the mean circulation. The spatial pattern of the first mode consists of high SSH in the offshore area, separated from high SSH next to the coast (south of 30°N) by low SSH in the core of the CCS. When the seasonal cycles of gradients are removed, the high SSH band next to the coast becomes the dominant feature. Thus the positive SSH anomalies during the second half of 1997 and early 1998 (clearest in the nonseasonal signal, Figure 9b) create the observed El Niño pattern of high sea level and poleward velocities next to the coast, strongest in the south. These patterns also occur during most winters, reversing in spring and early summer, as shown by the harmonic fits (Figure 9a). The nonseasonal time series (Figure 9b) makes clear the negative anomalies (low sea level and stronger equatorward flow) during the 1999

La Niña and again in 2001, while the values are near normal during 2000.

[31] The second and third EOFs for SSH contribute another 15% of the monthly SSH variance (Figures 9c and 9e). The spatial patterns for the second and third EOFs look more like the April and October SSH fields, respectively (Figures 4d and 4e), emphasizing the seasonally recurring eddies to the west of Point Eugenia. Fits to the harmonics produce peaks in March–June for the second mode and in August–November for the third mode, reaffirming their similarity to the April and October fields.

[32] If the three SSH modes are summed to reconstruct the most coherent part of the SSH variability, they account for only 30% of the total monthly SSH variance. The sum of the variance explained by the harmonic fits to the three time series accounts for only 7% of the total seasonal anomaly variance, revealing the very weak seasonal cycle of gradients in SSH and equatorward flow in the California Current off Baja California. This can also be seen in Figure 4f, where the amount of variance explained by the harmonic fits is high only at isolated points with values of 30–40%. On average, it explains only 8% of the seasonal anomaly variance. This weak seasonal cycle of SSH gradients can be characterized as poleward flow next to the coast, starting in late summer and fall (negative values

Sea Surface Height

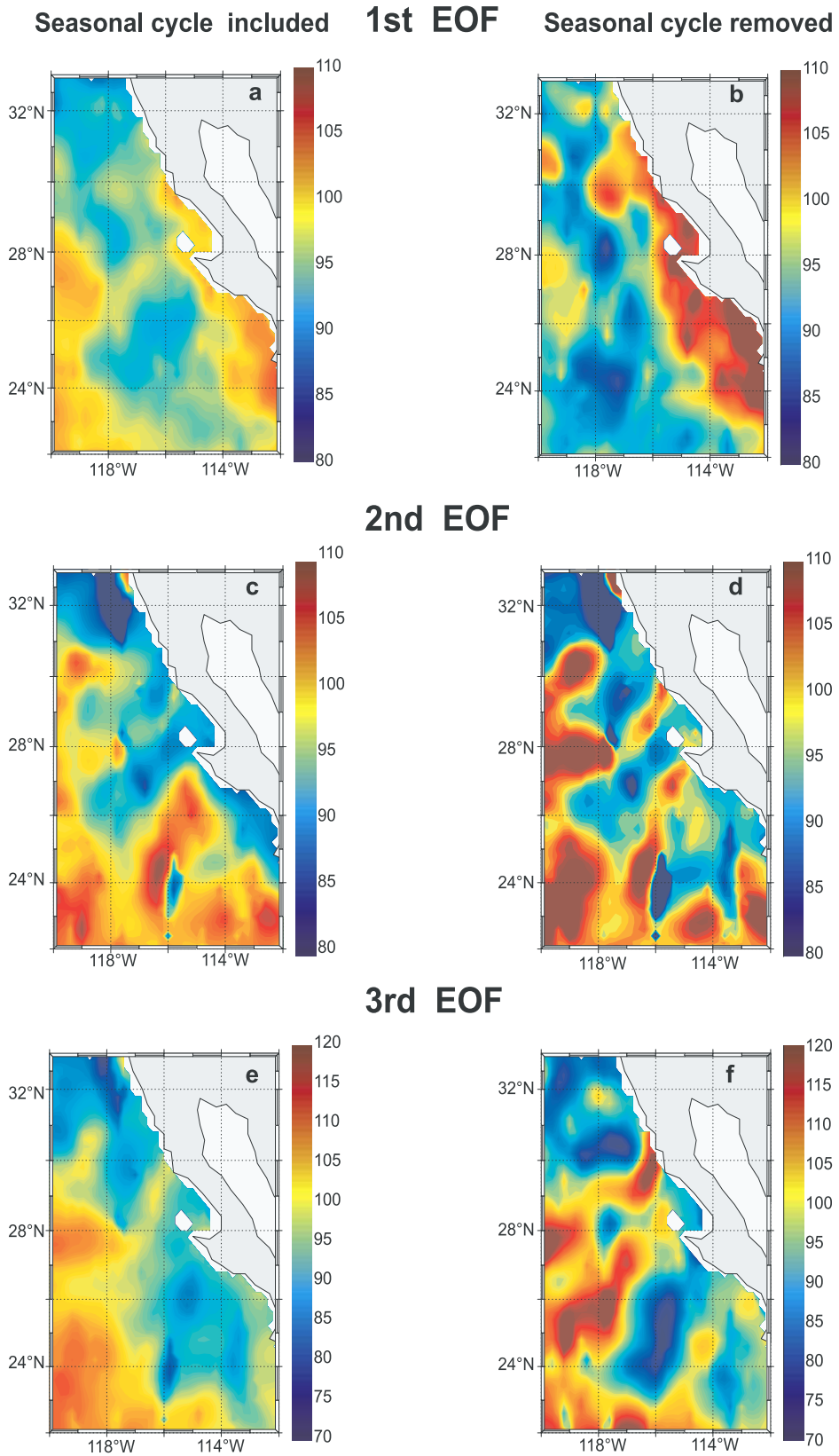


Figure 8.

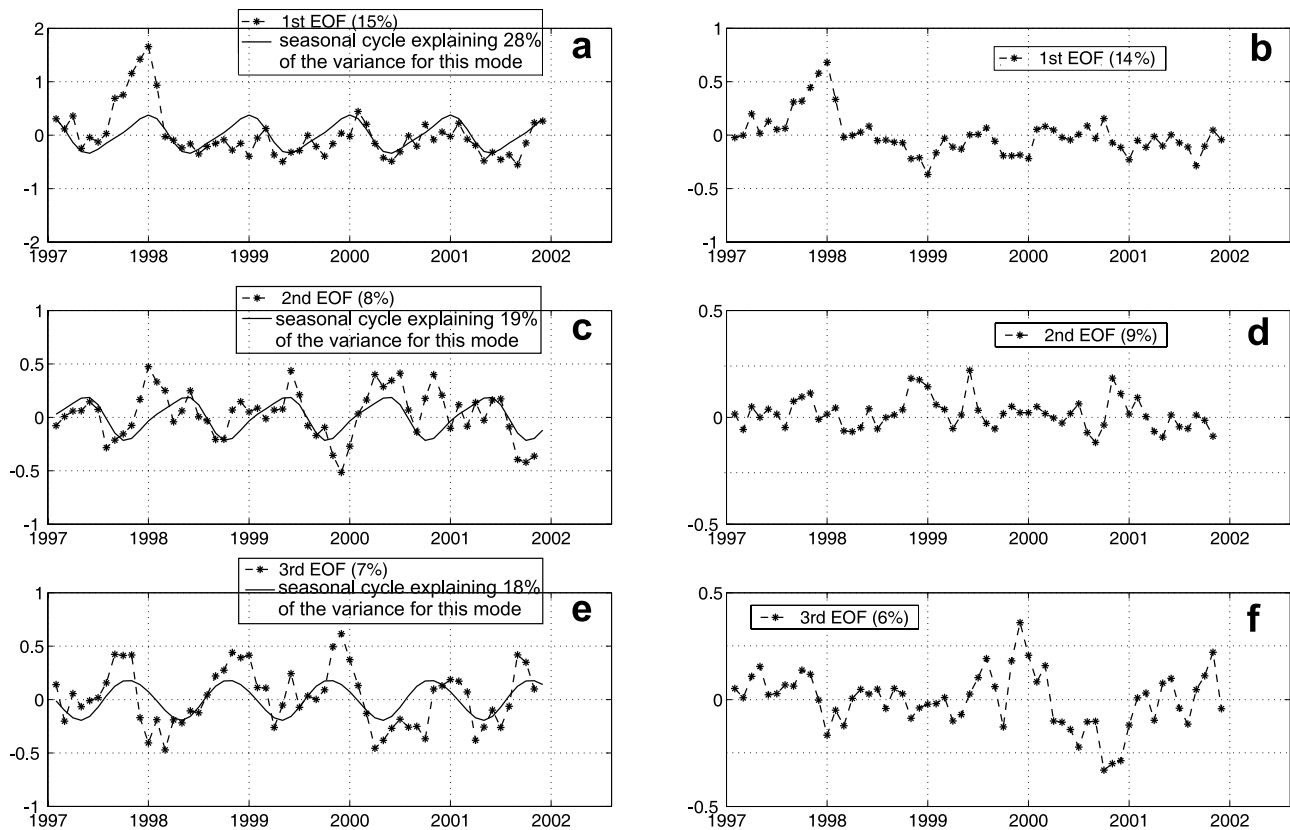


Figure 9. Time series of the first three EOF modes of sea surface height (SSH in relative units) during January 1997 to November 2001. First mode with (a) the harmonic seasonal cycle included and (b) the seasonal cycle removed. Second mode with (c) the harmonic seasonal cycle included and (d) the seasonal cycle removed. Third mode with (e) the harmonic seasonal cycle included and (f) the seasonal cycle removed.

for the second EOF) and reaching its maximum value south of 30°N in early winter (positive values of the first EOF), switching to equatorward flow in spring and summer (negative first EOF, positive second and third EOFs). Of the nonseasonal anomaly SSH fields, the first EOF shows the ENSO effects, with positive SSH anomalies (poleward flow) during the second half of 1997, switching by mid-1998 to negative anomalies (equatorward flow) for much of mid-1998 through 1999.

[33] Considering SST (Figures 10 and 11), the first mode alone accounts for 88% of the seasonal anomaly variance. However, although the second and third modes account for only 2% and 1% of the variance, their time series are reasonably well represented by harmonic seasonal cycles, their spatial patterns are coherent and they act to modulate the seasonal cycle seen in the first EOF in a meaningful manner. When the seasonal cycle is not removed, the harmonic fits represent 75% of the variability in the first EOF (66% of the total variance; adding the second and third harmonic fits explains only 1% more). The seasonal vari-

ability is dominated by an annual component, representing seasonal heating. It reaches a strong maximum at the end of the heating cycle in August–September, and a minimum at the end of the cooling cycle in early spring (March–April). The spatial pattern of this SST mode is positive everywhere (no zero crossing), with maximum values ($>5^{\circ}\text{C}$) next to the coast south of Point Eugenia, lower values ($>3.5^{\circ}\text{C}$) next to the coast north of Point Eugenia, and minimum values ($>2^{\circ}\text{C}$) offshore. Thus, when the time series is negative during February–June (the peak upwelling season), the region south of Point Eugenia is generally coldest, the region next to the coast north of Punta Eugenia is cool, and the offshore region is least cool (but all have seasonally cooled). When the time series is positive in July–November (the weaker upwelling season), this pattern is reversed, resulting in changes of up to 10°C south of Point Eugenia. This structure is in agreement with *Gallaudet and Simpson* [1994], representing the strong seasonal/interannual SST cycle observed in the California Current System [*Lynn et al.*, 1982; *Lynn and Simpson*, 1987].

Figure 8. Spatial patterns of the first three EOF modes of sea surface height (SSH in cm), from January 1997 to November 2001. A long-term mean dynamic height relative to 0/500 m (Figure 2b) has been added from *Levitus et al.* [1998] climatology. First mode with (a) the seasonal cycle included and (b) the seasonal cycle removed. Second mode with (c) the seasonal cycle included and (d) the seasonal cycle removed. Third mode with (e) the seasonal cycle included and (f) the seasonal cycle removed.

Sea Surface Temperature

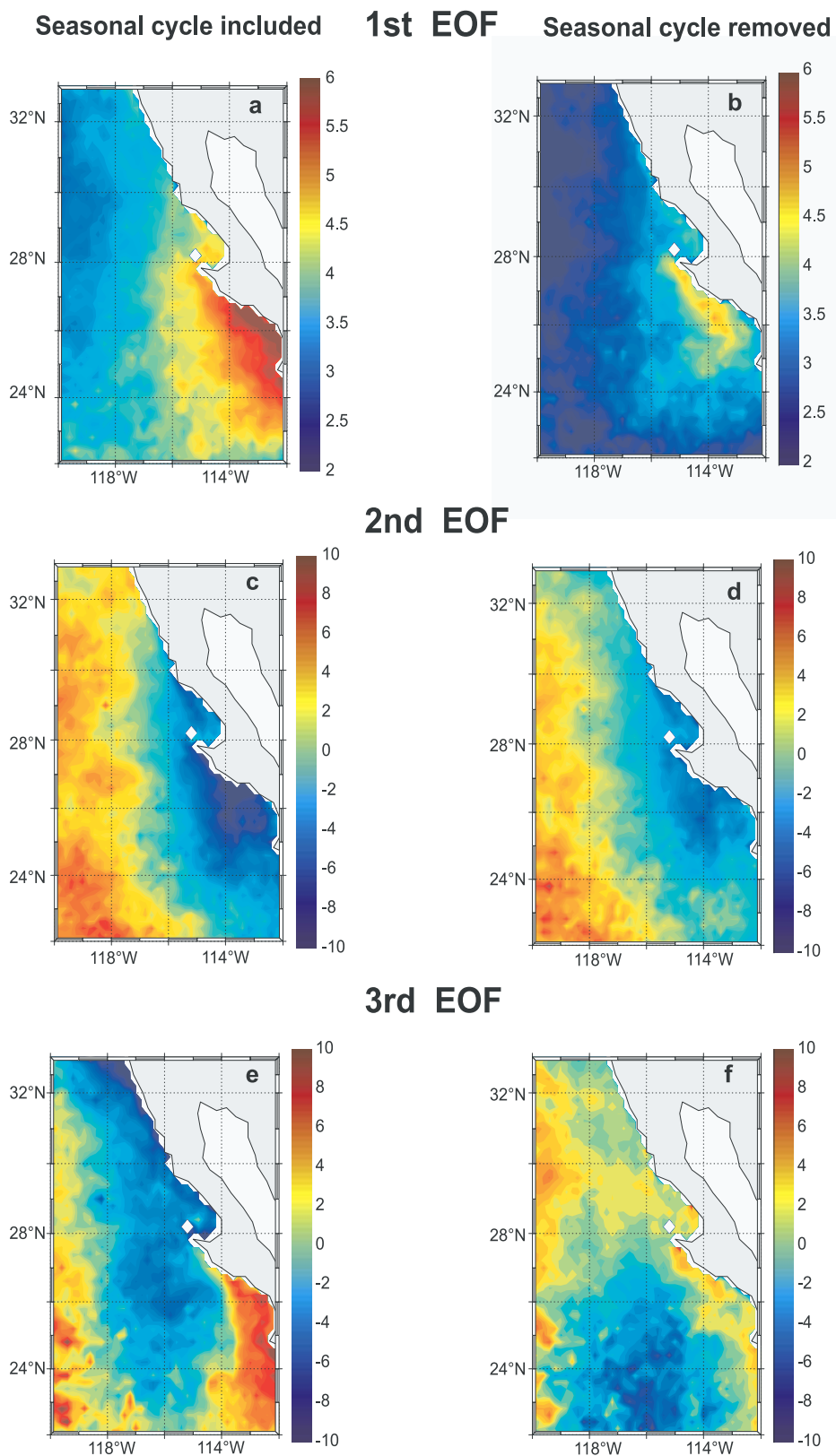


Figure 10. Spatial pattern of the first-three EOFs modes of sea surface temperature (SST in °C) from January 1997 to May 2002. First mode with (a) the seasonal cycle included and (b) the seasonal cycle removed. Second mode with (c) the seasonal cycle included and (d) the seasonal cycle removed. Third mode with (e) the seasonal cycle included and (f) the seasonal cycle removed.

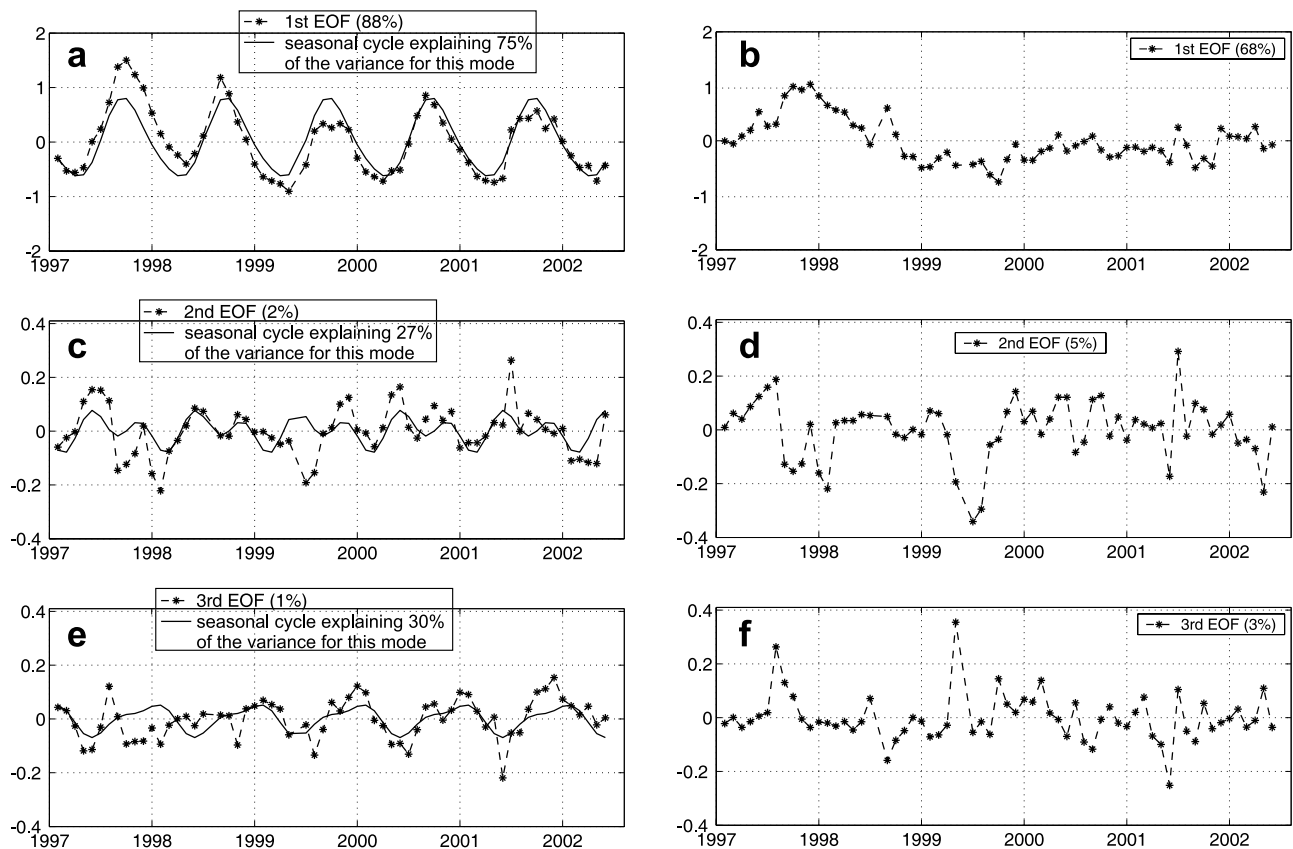


Figure 11. Time series of the first three EOF mode of sea surface temperature (SST in relative units) from January 1997 to May 2002. First mode with (a) the harmonic seasonal cycle included and (b) the seasonal cycle removed. Second mode with (c) the harmonic seasonal cycle included and (d) the seasonal cycle removed. Third mode with (e) the harmonic seasonal cycle included and (f) the seasonal cycle removed.

[34] As with SSH, the time series for the first SST mode is most positive during the El Niño, which is more evident in the time series when the seasonal signal is removed (Figures 10b and 11b). The El Niño warming off Baja California is strongest from August 1997 to March 1998, with the strongest SST anomalies of about 4°C concentrated along the coast south of Point Eugenia between 25°N and 28°N . The La Niña influence off Baja California is also captured by the first nonseasonal EOF, with SST anomalies around -2°C (Figures 10b and 11b). During the last 3 years of our data, especially during 2000, SST as represented by the first EOF remained slightly negative but close to the seasonal cycle.

[35] The second EOF of SST seasonal anomalies describes cool water around and south of Point Eugenia with semiannual peaks in May–July and November–December. Its effect is to maintain cool water around Point Eugenia as the overall area experiences seasonal warming and upwelling decreases in June–July (Figures 10c and 11c). The second nonseasonal EOF explains 5% of the nonseasonal variance and again represents cool water around and south of Point Eugenia (warmer when the time series is negative during the El Niño and in mid-1999). This pattern contributes several periods of cooler water during 2000. The zero line extends along the core of the California Current, allowing the temperature difference between the coast and offshore to

increase and decrease. The third seasonal mode of temperature (Figures 10e and 11e) explains only 1% of variance, but represents the spatial pattern of cool water advection from the north in the core of the CCS. It is positive during fall and winter (following the strong cool advection in summer), becoming negative in April–May (after the minimum of cool advection or the occurrence of warm advection from the south in winter).

3.5. Qualitative Correlation Analyses

[36] A standard method used to quantify the degree of local upwelling forcing and response is to calculate correlations between the CUI time series and the first EOF time series of the other variables. When the seasonal cycles are not removed, the correlation coefficients between the seasonal anomalies of the CUI on one hand and seasonal anomalies of SST, pigment concentrations, and SSH are -0.47 , 0.37 , and -0.31 , respectively. These correlations are qualitatively as expected for seasonal upwelling coastal ocean systems. For each EOF, positive time series corresponds to positive values next to the coast, so these relationships show that stronger upwelling-favorable winds in spring are coincident with lower temperatures, higher pigments, and lower SSH next to the coast. No causal relationship can be inferred from the correlations, since the presence of the seasonal cycles artificially increases

the correlations and makes the determination of statistical significance problematic [Chelton, 1982]. Removing the seasonal cycles results in reduced values of the correlations and marginally significant correlations between increased upwelling forcing and lower SST and SSH (with correlation coefficients of -0.29 and -0.23 , respectively). There is no relation between nonseasonal time series of the CUI and first EOF pigment concentrations.

[37] When pigment concentrations are directly correlated with SST and SSH, the relationships between seasonal anomaly time series are again as expected. Correlation coefficients between CHL and SST or SSH are -0.49 or -0.33 , respectively, showing the presence of high pigment concentrations for conditions when SST and SSH are low. These relationships again weaken to the point of insignificance for the time series of nonseasonal anomalies.

[38] Relating nonseasonal monthly chlorophyll pigment fields to local forcing is always a perplexing problem [Strub *et al.*, 1990], and a number of problems with these comparisons could be named. In this case, however, the simplest reason for the low nonseasonal correlations is the presence of El Niño signals in the relatively short time series (Figures 7b, 9b, and 11b). These signals increase SSH and deepen the pycnocline and nutricline, indirectly decreasing nutrients and pigment concentrations, although wind stress anomalies remain upwelling-favorable during the El Niño (Figure 5b). Following the El Niño, the time series show that SSH and SST anomalies were low and pigment concentrations were high during 1999, when the CUI anomaly was positive (La Niña?); however, pigment concentration anomalies were also high in 2000 and part of 2001, when the CUI anomaly was mostly negative. Thus, during this 4- to 5-year period off Baja California, the “local” monthly wind stress anomalies are simply not the dominant factor controlling monthly pigment concentration anomalies.

3.6. Chlorophyll Concentrations off Baja California During the El Niño

[39] Previous descriptions of the region off Baja California during the El Niño have characterized its reduced mesoscale activity and increased poleward surface flow [Durazo and Baumgartner, 2002]. This results in an inflow of warm Subtropical Surface Water (StSW) from the south and offshore, high SSH, and poor nutrients due a deepened nutricline [Chávez *et al.*, 2002; Collins *et al.*, 2002; Lynn and Bograd, 2002; Strub and James, 2002]. The timing of the El Niño effects at the eastern equatorial Pacific is well established, with two periods of high SSH, depressed isotherms, and increased SST: May–July and October–December 1997 [Chavez *et al.*, 1998; McPhaden, 1999]. The timing of the arrival of the signal in the CCS depends on the variable examined.

[40] The EOF time series of chlorophyll in Figures 7a and 7b from SeaWiFS suggests that the El Niño event off Baja California was in place by January 1998 and extended to July 1998, with a transition to La Niña conditions during August 1998 to January 1999. Kahru and Mitchell [2000] report a similar temporal progression. Unfortunately, the SeaWiFS data are not available before September 1997 to document the transition into El Niño conditions. In the SSH EOF time series (Figures 9a and 9b), the El Niño event

starts in August 1997 and ends in February 1998, with a transition period to La Niña from February to September 1998. The SST EOF time series (Figures 11a and 11b) shows a smoother increase and warm SST anomalies between mid-1997 to mid-1998. Lynn *et al.* [1998] and Durazo and Baumgartner [2002] proposed that the El Niño effects in our study area were present by October 1997, using hydrographic temperature and salinity data. In a larger scale study, Strub and James [2002] show a rapid movement of high altimeter SSH anomalies from the equator to the Gulf of California in May–June 1997, followed by a more gradual progression up the coast of Baja California in July–August. The end of the El Niño was even more dramatic than the beginning. Kahru and Mitchell [2001] used satellite SST fields to demonstrate an abrupt change in 1998 from one of the warmest months (since 1981) to one of the coldest months in their 20-year SST time series. The influence of La Niña event was evident during all of 1999 in all the time series (Figures 7a, 7b, 9a, 9b, 11a, and 11b), diminishing its influence after that.

[41] Since our primary interest is in the phytoplankton signal, we provide a more complete view of the progression during the El Niño by using monthly nonseasonal anomalies of surface chlorophyll concentrations from September 1997 through August 1998 (Figure 12). These anomalies are formed by removing the seasonal cycle, (as in equation (1)) from the time series. During September 1997, there are positive anomalies ($>0.3 \text{ mg m}^{-3}$) at inshore locations north of Point Eugenia (28°N – 30°N) (Figure 12a). In October, anomalies increased in area and magnitude to $>0.6 \text{ mg m}^{-3}$ and moved slightly to the north and offshore of San Quintin (Figure 12b). Although this movement may represent displacement of positive anomalies by an inflow from the south, it looks like a local process without connection to high values of pigment farther south. High chlorophyll values off San Quintin have been reported during October for other years [Peláez and McGowan, 1986; Aguirre-Hernández *et al.*, 2004]. Phytoplankton species composition during October 1997 in this region of high pigment concentrations were dominated mainly by dinoflagellates and diatoms ($\sim 10^5 \text{ cells L}^{-1}$) (C. Bazán-Guzmán *et al.*, Distribución de los principales grupos fitoplanctónicos y protozoarios en aguas adyacentes a la península de Baja California (in Spanish), CICESE technical report, in preparation, 2004). This suggests an advanced stage of ecosystem succession, which should be followed by lower nutrient concentrations. However, it is also possible that the increase in phytoplankton biomass during October and subsequent months is related to strong “Santana” winds, carrying dust and micronutrients to the ocean from the Baja California desert. These winds are common in the region from September to November, and their effects during February 2002 are well described by Castro *et al.* [2003].

[42] During November 1997 to March 1998 (Figures 12c to 12g), positive pigment anomalies of $\sim 0.2 \text{ mg m}^{-3}$ occur in the offshore region, while negative anomalies develop next to the coast and reach values of $<-0.8 \text{ mg m}^{-3}$ during March to July 1998 (Figures 12g to 12k). By August 1998 (Figure 12l), the nearshore negative pigment anomalies began to decrease in magnitude. Kahru and Mitchell [2000, 2002] examined these anomalously high offshore pigment concentrations and hypothesized that phytoplankton

Chlorophyll

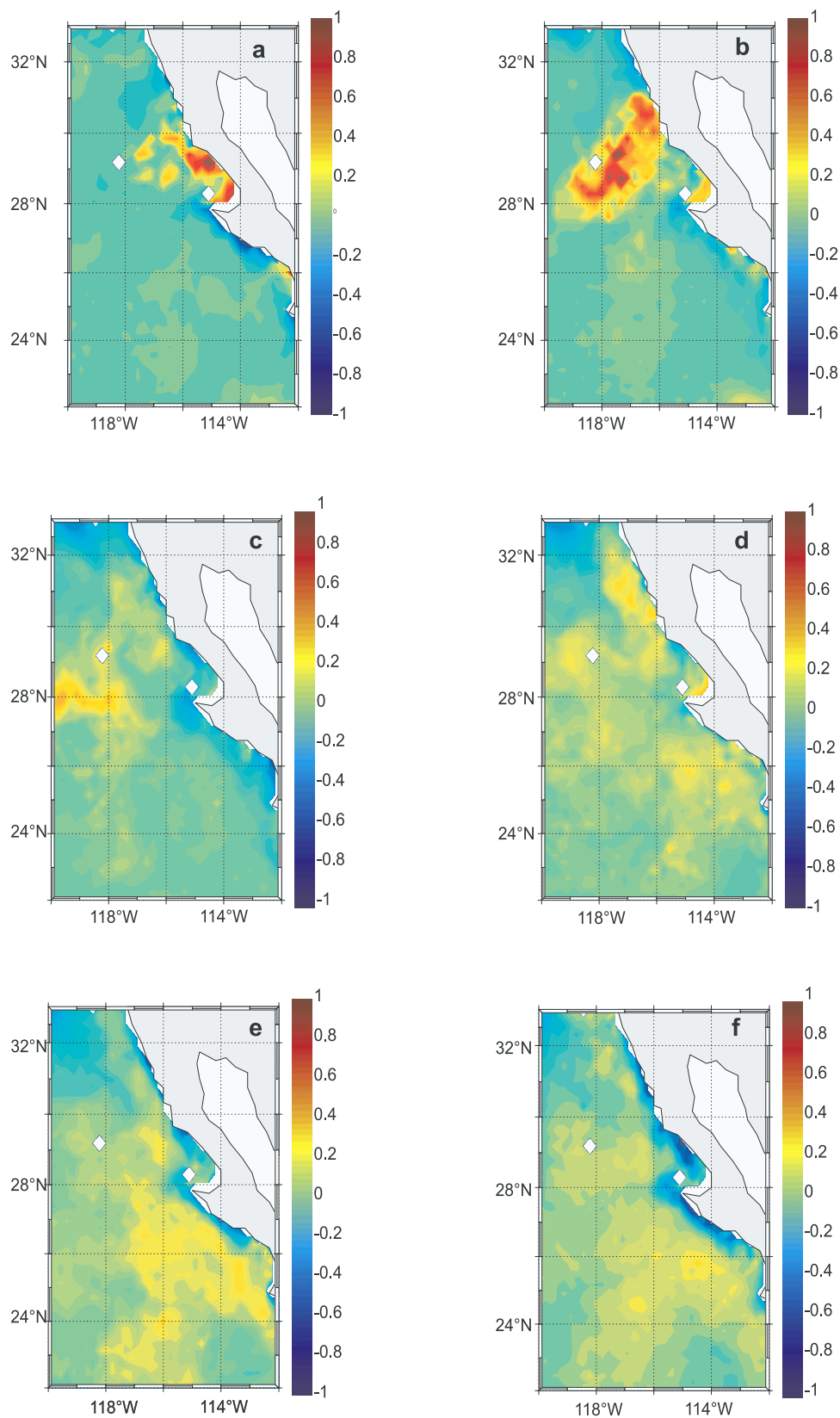


Figure 12. Nonseasonal chlorophyll concentration anomalies (mg m^{-3}) during the El Niño from September 1997 to August 1998. (a) September, (b) October, (c) November, (d) December, (e) January, (f) February, (g) March, (h) April, (i) May, (j) June, (k) July, and (l) August.

Chlorophyll

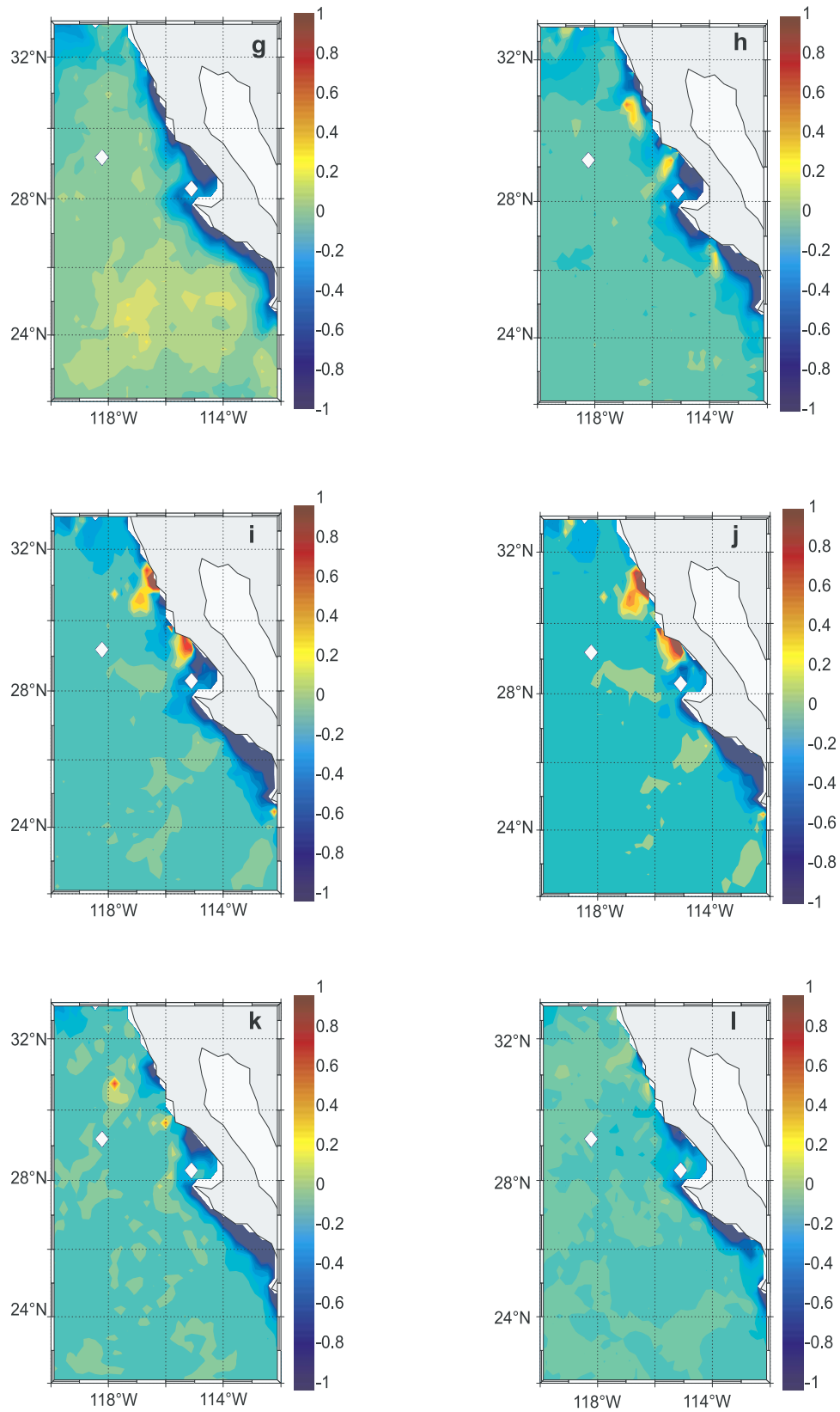


Figure 12. (continued)

assemblages in the warm and stratified offshore waters were caused by nitrogen-fixing cyanobacteria. However, blooms of *Trichodesmium* do not usually produce strong anomalies in satellite-derived pigment concentrations. *Subramaniam et al.* [2002] show that standard ocean color chlorophyll algorithms would underestimate *Trichodesmium*-specific chlorophyll by a factor of at least 4, due to self-shading by the colonies. This suggests that other phytoplankton communities may have been present, interacting with the cyanobacteria to enhance the positive anomalies in the offshore region. Hypotheses for the source of the elevated pigment anomalies (whatever the species) include advection of phytoplankton or nutrients from the north or from offshore. Advection from farther north might imply that the equatorward California Current was displaced offshore by water intruding next to the coast from the south. Advection from offshore might include nutrients that were raised into the euphotic zone by the increased Ekman suction caused by storms associated with atmospheric El Niño conditions. The source of the offshore pigment anomalies remains to be definitively determined.

4. Conclusions

[43] 1. The seasonal variability in satellite-derived chlorophyll pigment concentrations, sea surface height, and sea surface temperature is estimated off Baja California between 22°N and 34°N using harmonic fits and EOFs for time series spanning 4–5 years (1997 to late 2001 for SSH, 1997 to mid-2002 for SST, and 1998 to mid-2002 for pigment). These help to identify three dynamic regions off Baja California: an upwelling zone next to the coast, the Ensenada Front in the north (in the Southern California Bight), and regions of repeated meanders and/or eddy variability west and southwest of Punta Eugenia (Figures 4 and 6–11).

[44] 2. The seasonal cycles explain the most variance for SST over a broad offshore area and explain the least variance for SSH. The seasonal cycle for pigment concentrations is more confined to a narrow (<50 km) coastal region than for SST and SSH (Figures 4 and 6–7). The timing of the seasonal changes strongly implicates upwelling-favorable winds as the driving force over seasonal timescales. On nonseasonal timescales, however, changes in the monthly wind anomalies do not appear to be the primary source of variability in the oceanic parameters, especially not in monthly anomalies of surface chlorophyll pigment concentrations.

[45] 3. Features in coastal geometry (capes and bays, especially the presence of Point Eugenia), appear to play an important role in the alongshore spatial patterns of the first three EOF modes of seasonal and nonseasonal of chlorophyll pigment concentration (Figure 6). Point Eugenia also appears to affect the seasonal and nonseasonal EOF patterns in SST (Figures 4 and 10). A dominant eddy pair develops seasonally west of Point Eugenia, one of the few places where the harmonic seasonal cycle accounts for as much of 40% of the SSH variance (Figures 4 and 8).

[46] 4. In the study area, the strongest effects are seen in the coastal region during the El Niño, with weaker effects during La Niña (Figures 6b, 7b, 8b, 9b, 10b, and 11b). These effects are one of the sources of the low correlations between nonseasonal anomalies of wind-forcing (monthly

CUI anomalies) and the nonseasonal EOFs of pigment concentration anomalies.

[47] 5. Chlorophyll pigment concentrations in the offshore region can be positive during El Niño conditions, as they were in 1998 (Figure 12), for reasons not presently known.

[48] The coastal upwelling zone identified in the first conclusion above is the most inshore of three regions defined by the temporal mean of the satellite chlorophyll pigment concentrations off Baja California during 1998–2002 (Figure 2a): an inshore eutrophic area, an oligotrophic offshore region, and an intermediate mesotrophic zone. High pigment concentrations are also found in the region north of the Ensenada Front.

[49] The long-term mean dynamic height (Figure 2b) has lower values (≤ 90 cm) next to the coast, consistent with upwelling of dense water, and highest values offshore (≥ 105 cm). SSH isopleths of constant height are roughly parallel to the coast, indicating a current toward the southeast (the California Current). North of 31°N, there is a region of low SSH, a signature of anticyclonic recirculation in the Southern California Bight north of the Ensenada Front.

[50] The mean field of SST (Figure 2c) shows a north-south gradient, approximately perpendicular to the coast. Unlike the other mean fields, the north-south gradient in the mean SST field indicates control by surface processes, in this case surface heating with a strong latitudinal gradient.

[51] Seasonal anomalies of chlorophyll concentrations (Figures 4 and 6) show a spatial distribution similar to the mean distribution, again identifying the coastal upwelling band with maximum values (up to 0.5 mg m^{-3}) during April and near-zero values in the offshore region (second conclusion). Seasonal anomalies of SST (Figure 4 and 10) are negative in a coastal region in April, but not restricted to as narrow a coastal band as chlorophyll concentrations. The seasonal anomalies in SST are especially strong near and to the south of Point Eugenia. SSH anomalies (Figures 4 and 8) also show a spatial distribution with high amplitudes against the coast, but less concentrated than chlorophyll concentrations. The coastal SSH anomalies are low next to the coast in April and highest around October.

[52] These seasonal patterns are consistent with the mean pattern of seasonal forcing by ECMWF winds during 1986–98. Over the ocean, the mean wind field is favorable for upwelling next to the coast over the entire study region (Figure 3). These winds have a seasonal upwelling-favorable maximum in early spring and a minimum in fall, but do not reverse over the ocean. The coincident timing of extremes of forcing and responses in April, typical of upwelling systems, leads us to identify the prime source of seasonal changes in pigment concentrations, SST and SSH as the equatorward winds (second conclusion). The seasonal cycles of chlorophyll concentrations and SST are strong (explaining 42% and 66% of the total variance), while the seasonal cycle of SSH is weak (explaining only 4% of the total variance).

[53] The spatial patterns for seasonal changes in SSH include cyclonic and anticyclonic meanders or eddies to the west and southwest of Point Eugenia (Figures 4 and 8), the third region identified in the first conclusion. Further evidence for repeated eddies in this region is provided by the seasonal cycle for SST, which explains least variance in a narrow coastal region and along the hypothesized path of

eddies to the west and southwest of Point Eugenia (Figure 4i). We hypothesize that this is due to the short timescales for these events in the SST signal and their irregular sampling due to clouds. Next to the coast, the spatial patterns of EOFs for SST and pigment concentration anomalies suggests control by the time-invariant coastal geometry, as does the similarity between patterns in the seasonal and nonseasonal EOFs. This and the region of eddy activity off Point Eugenia support the third conclusion.

[54] When the seasonal cycles are removed, the largest signals are those of the ENSO variability, with El Niño (La Niña) effects characterized by high (low) sea surface height, warm (cold) SST, and low (high) chlorophyll concentrations next to the coast. Mechanisms that cause La Niña conditions are not as well understood as El Niño. Nonseasonal anomalies were dominated by cold conditions following the El Niño in 1999–2001, especially during 1999. Nonseasonal wind anomalies during El Niño can remain upwelling-favorable, and during La Niña they can be either upwelling- or downwelling-favorable. This is a major cause for low correlations between nonseasonal time series of winds and chlorophyll pigment concentrations (second and fourth conclusions).

[55] The nonseasonal fields of pigment concentrations suggest an offshore movement of high pigment concentrations in September–October 1997, followed by positive chlorophyll anomalies in the offshore region between November 1997 and March 1998. Even stronger negative pigment concentrations anomalies occur next to the coast during January–August 1998. The negative anomalies persist longest south of Point Eugenia. Several possible hypotheses have been suggested for the positive offshore pigment anomalies during the El Niño, but none have been confirmed or eliminated at this time (fifth conclusion).

[56] **Acknowledgments.** The first author had a fellowship from CONACyT, Mexico, and support through projects Fase I, Oceanografía por Satélite (225080-5-4302PT; DAI J002/750/00), G-35326, CICESE (Ecology Department), IAI-CRN 062, IOCCG, and COAS-OSU (NAS5-31360, OCE-9907854). SeaWiFS chlorophyll pigment data were processed and made available by Andrew Thomas, at the University of Maine. Altimeter data came from the NOAA-NASA Pathfinder project. SST data was collected by Ocean Imaging, Inc., and archived at Oregon State University, as part of the U.S. GLOBEC NEP project, with support from NSF grant OCE-0000900. This is contribution number 422 of the U.S. GLOBEC program, jointly funded by the National Science Foundation and the National Oceanic and Atmospheric Administration. This is also a contribution of the IMECOCAL-CICESE research program to the scientific agenda of the Eastern Pacific Consortium of the InterAmerican Institute for Global Change Research (IAI-EPCOR). J.M. Dominguez drafted the final figures.

References

- Abbott, M. R., and B. Barksdale (1991), Phytoplankton pigment patterns and wind forcing off central California, *J. Geophys. Res.*, **96**, 14,649–14,667.
- Aguirre-Hernández, E., G. Gaxiola-Castro, S. Nájera-Martínez, T. Baumgartner, M. Kahru, and B. G. Mitchell (2004), Phytoplankton absorption, photosynthetic parameters, and primary production off Baja California, summer and autumn 1998, *Deep Sea Res., Part II*, in press.
- Bakun, A. (1975), Daily and weekly indices, west coast of North America, 1967–1973, *NOAA Tech. Rep., NMFS SSRF-693*.
- Barnes, R. A., A. W. Holmes, W. L. Barnes, W. E. Esaias, C. R. McClain, and T. Svitek (1994), SeaWiFS Prelaunch Radiometric Calibration and Spectral Characterization, *NASA Tech. Memo.*, 104566, 55 pp.
- Barth, J. A., S. D. Piece, and R. L. Smith (2000), A separating upwelling coastal jet at Cape Blanco, Oregon and its connection to the California Current System, *Deep Sea Res., Part II*, **47**, 783–810.
- Bernal, P. A. (1981), A review of the low-frequency response of the pelagic ecosystem in the California Current, *Calif. Coop. Ocean. Fish. Invest. Rep.*, **22**, 49–62.
- Bograd, S. J., et al. (2000), The state of the California Current, 1999–2000: Forward to a new regimen?, *Calif. Coop. Ocean. Fish. Invest. Rep.*, **41**, 26–52.
- Castro, R., A. Parés-Sierra, and S. G. Marinone (2003), Evolution and extension of the Santa Ana winds of February 2002 over the ocean, off California and the Baja California Peninsula, *Cienc. Mar.*, **29**, 275–281.
- Chávez, F. P. (1996), Forcing and biological impact of onset of the 1992 El Niño in central California, *Geophys. Res. Lett.*, **23**, 265–268.
- Chávez, F. P., P. G. Strutton, and M. J. McPhaden (1998), Biological-physical coupling in the central equatorial Pacific during the onset of the 1997–1998 El Niño, *Geophys. Res. Lett.*, **25**, 3543–3546.
- Chávez, F. P., J. T. Pennington, C. G. Castro, J. P. Ryan, R. P. Michisaki, B. Schlining, P. Walz, K. R. Buck, A. McFadyen, and C. A. Collins (2002), Biological and chemical consequences of the 1997–1998 El Niño in central California waters, *Prog. Oceanogr.*, **54**, 205–232.
- Chelton, D. B. (1982), Statistical reliability and the seasonal cycle: Comments on “Bottom pressure measurements across the Antarctic Circumpolar Current and their relation to the wind,” *Deep Sea Res.*, **29**, 1381–1388.
- Chelton, D. B. (1984), Seasonal variability of alongshore geostrophic velocity off central California, *J. Geophys. Res.*, **89**, 3473–3486.
- Collins, C. A., C. G. Castro, H. Asanuma, T. A. Rago, S.-K. Han, R. Durazo, and F. P. Chávez (2002), Changes in the hydrography of Central California waters associated with the 1997–98 El Niño, *Prog. Oceanogr.*, **54**, 129–147.
- Durazo, R., and T. R. Baumgartner (2002), Evolution of oceanographic conditions off Baja California, 1997–1999, *Prog. Oceanogr.*, **54**, 7–31.
- Durazo, R., et al. (2001), The state of the California Current, 2000–2001: A third straight La Niña year, *Calif. Coop. Ocean. Fish. Invest. Rep.*, **42**, 29–60.
- Fargion, G. S., J. A. McGowan, and R. H. Stewart (1993), Seasonality of chlorophyll concentrations in the California Current: A comparison of two methods, *Calif. Coop. Ocean. Fish. Invest. Rep.*, **34**, 35–50.
- Gallaudet, T. C., and J. J. Simpson (1994), An empirical orthogonal function analysis of remotely sensed sea surface temperature variability and its relation to interior oceanic processes of Baja California, *Remote Sens. Environ.*, **47**, 375–389.
- Gaxiola-Castro, G., and S. Alvarez-Borrego (1991), Relative assimilation numbers of phytoplankton across a seasonally recurring front in the California Current off Ensenada, *Calif. Coop. Ocean. Fish. Invest. Rep.*, **32**, 91–96.
- Gómez-Valdés, J., and H. Vélez-Muñoz (1982), Variación estacional de temperatura y salinidad en regiones costeras de la Corriente de California, *Cienc. Mar.*, **8**, 167–176.
- Haidvogel, D. B., A. Beckmann, and K. S. Hedstrom (1991), Dynamical simulations of filament formation and evolution in the coastal transition zone, *J. Geophys. Res.*, **96**, 15,017–15,040.
- Haurv, I. R., E. Venrick, C. L. Fey, J. A. McGowan, and P. P. Niiler (1993), The Ensenada Front: July 1985, *Calif. Coop. Ocean. Fish. Invest. Rep.*, **34**, 69–88.
- Hayward, T. L., et al. (1999), The state of the California Current, 1998–1999: Transition to cool-water conditions, *Calif. Coop. Ocean. Fish. Invest. Rep.*, **40**, 29–62.
- Hickey, B. M. (1979), The California Current System—Hypotheses and facts, *Prog. Oceanogr.*, **8**, 191–279.
- Hickey, B. M. (1998), Coastal oceanography of western North America from the tip of Baja California to Vancouver Island, *Sea*, **11**, 345–393.
- Huyer, A. (1983), Coastal upwelling in the California Current System, *Prog. Oceanogr.*, **12**, 259–284.
- Ikeda, M., and W. J. Emery (1984), Satellite observations and modeling of meanders in the California Current System off Oregon and northern California, *J. Phys. Oceanogr.*, **14**, 1434–1450.
- Kahru, M., and G. Mitchell (2000), Influence of 1997–1998 El Niño on the surface chlorophyll in the California Current, *Geophys. Res. Lett.*, **27**, 2937–2940.
- Kahru, M., and G. Mitchell (2001), Seasonal and nonseasonal variability of satellite-derived chlorophyll and colored dissolved organic matter concentration in the California Current, *J. Geophys. Res.*, **106**, 2517–2529.
- Kahru, M., and B. G. Mitchell (2002), Influence of the El Niño–La Niña cycle on satellite-derived primary production in the California Current, *Geophys. Res.*, **29**(17), 1846, doi:10.1029/2002GL014963.
- Levitus, S., T. P. Boyer, M. E. Conkright, T. O’Brien, J. Antonov, C. Stephens, L. Stathopoulos, D. Johnson, and R. Gelfeld (1998), *World Ocean Database 998*, vol. 1, *Introduction*, NOAA Atlas NESDIS 18, Natl. Oceanic and Atmos. Admin., Silver Spring, Md.
- Lynn, R. J., and S. J. Bograd (2002), Dynamic evolution of the 1997–1999 El Niño–La Niña cycle in the southern California Current System, *Prog. Oceanogr.*, **54**, 59–75.

- Lynn, R. J., and J. J. Simpson (1987), The California Current System: The seasonal variability of physical characteristics, *J. Geophys. Res.*, **92**, 12,947–12,966.
- Lynn, R. J., K. A. Bliss, and L. E. Eber (1982), Vertical and horizontal distributions of seasonal mean temperature, salinity, sigma-t, stability, dynamic height, oxygen and oxygen saturation in the California Current, 1950–1978, *Calif. Coop. Ocean. Fish. Invest. Atlas*, **30**, 513 pp.
- Lynn, R. J., et al. (1998), The State of California Current, 1997–1998: Transition to El Niño conditions, *Calif. Coop. Ocean. Fish. Invest. Rep.*, **39**, 25–49.
- McCarthy, J. J., A. R. Robinson, and B. J. Rothschild (2002), Introduction-biological-physical interactions in the sea: Emergent findings and new directions, in *The Sea*, vol. 12, edited by A. R. Robinson, J. J. McCarthy, and B. J. Rothschild, pp. 1–16, John Wiley, New York.
- McGowan, J. A., D. B. Chelton, and A. Conversi (1996), Plankton pattern, climate and change in the California Current, *Calif. Coop. Ocean. Fish. Invest. Rep.*, **37**, 45–68.
- McPhaden, M. J. (1999), Genesis and evolution of the 1997–1998 El Niño, *Science*, **283**, 950–954.
- Narimousa, S., and T. Maxworthy (1989), Applications of a laboratory model to the interpretation of satellite and field observations of coastal upwelling, *Dyn. Atmos. Oceans*, **13**, 1–46.
- Olson, D. B. (2002), Biophysical dynamics of ocean fronts, in *The Sea*, vol. 12, edited by A. R. Robinson, J. J. McCarthy, and B. J. Rothschild, pp. 188–218, John Wiley, Hoboken, N.J.
- Parés-Sierra, A., W. B. White, and C. K. Tai (1993), Wind-driven coastal generation of annual mesoscale eddy activity in the California Current System: A numerical model, *J. Phys. Oceanogr.*, **23**, 1110–1121.
- Parés-Sierra, A., M. López, and E. Pavía (1997), Oceanografía Física del Océano Pacífico Nororiental, in *Contribuciones a la Oceanografía Física en México*, *Monogr. Ser.*, vol. 3, pp. 1–24, Unión Geofis. Mex., Puerto Vallarta, Mex.
- Peláez, J., and F. Guan (1982), California Current chlorophyll measurements from satellite data, *Calif. Coop. Ocean. Fish. Invest. Atlas*, **23**, 212–225.
- Peláez, J., and J. A. McGowan (1986), Phytoplankton pigment patterns in the California Current as determined by satellite, *Limnol. Oceanogr.*, **31**, 927–950.
- Schwing, F. B., M. O'Farrel, J. Steger, and K. Blaltz (1996), Coastal upwelling indices, west coast of North America 1946–1995, *NOAA Tech. Rep.*, *NMFS SWFSC-231*.
- Simpson, J. J., and R. J. Lynn (1990), A Mesoscale eddy dipole in the offshore California Current, *J. Geophys. Res.*, **95**, 13,009–13,022.
- Simpson, J. J., C. J. Koblinsky, J. Peláez, L. R. Haury, and D. Wiesenhahn (1986), Temperature–plant pigment–optical relations in a recurrent offshore mesoscale eddy near Point Conception, California, *J. Geophys. Res.*, **91**, 12,919–12,936.
- Soto-Mardones, L., A. Parés-Sierra, J. García, R. Durazo, and S. Hormazabal (2004), Analysis of the mesoscale structure in the IMECOCAL region (off Baja California) from Hydrographic, ADCP and Altimetry Data, *Deep Sea Res., Part II*, in press.
- Strub, P. T., and C. James (2002), The 1997–1998 Oceanic El Niño signal along the southeast and northeast Pacific boundaries—An altimetric view, *Prog. Oceanogr.*, **54**, 439–458.
- Strub, P. T., C. James, A. Thomas, and M. Abbot (1990), Seasonal and nonseasonal variability of satellite-derived surface pigments concentration in the California Current, *J. Geophys. Res.*, **95**, 11,501–11,530.
- Strub, P. T., P. M. Kosro, and A. Huyer (1991), The nature of cold filaments in the California Current System, *J. Geophys. Res.*, **96**, 14,743–14,768.
- Subramaniam, A., C. W. Brown, R. R. Hood, E. J. Carpenter, and D. G. Capone (2002), Detecting *Trichodesmium* blooms in SeaWiFS imagery, *Deep Sea Res., Part II*, **49**, 107–121.
- Thomas, A. C., and P. T. Strub (1990), Seasonal and interannual variability of pigment concentrations across a California Current frontal zone, *J. Geophys. Res.*, **95**, 13,023–13,042.
- Thomas, A. C., F. Huang, P. T. Strub, and C. James (1994), Comparison of the seasonal and interannual variability of phytoplankton pigment concentrations in the Peru and California Current systems, *J. Geophys. Res.*, **99**, 7355–7370.
- Venrick, E. L. (2000), Summer in the Ensenada Front: The distribution of phytoplankton species, July 1985 and September 1988, *J. Plankton Res.*, **22**, 813–841.

E. Beier, T. L. Espinosa-Carreón, G. Gaxiola-Castro, and F. Ocampo-Torres, Centro de Investigación Científica y de Educación Superior de Ensenada, Km 107 Carr. Tijuana-Ensenada, Ensenada, Baja California, Mexico. (ebeier@cicese.mx; lespinos@cicese.mx; ggaxiola@cicese; ocampo@cicese.mx)

P. T. Strub, College of Oceanic and Atmospheric Sciences, Oregon State University, 104 Ocean Administration Building, Corvallis, OR 97331-5503, USA. (tstrub@coas.oregonstate.edu)